

Investigation and Modelling of the Influence of Cooling Rates on the Microstructure of AZ91 Alloys

S. Gavras, M. U. Bilal, D. Tolnai, and N. Hort

Abstract

An increasingly important tool in modern experimental investigations is the ability to accurately produce a digital model or “digital twin” of samples and their properties. This goes hand-in-hand with the primary tenant of Industry 4.0 which is to provide advanced manufacturing solutions through the use of cyber-physical systems. A comparison of various quenching media, namely liquid nitrogen, water at 5 °C, water at 20 °C and in the air on the microstructure of permanent mould cast AZ91 alloys was investigated. Particular emphasis was centred on the changes in microstructural features such as grain size and dendrite arm spacing. Phase-field method was used to produce a digital twin and qualitative analysis of the investigated cooling rates on AZ91. The combination of practical microstructural investigations and the simulated microstructures will advance the knowledge of cooling rate influences on AZ91 and their ability to be accurately simulated to assist with property and microstructural predictions.

Keywords

AZ91 • Quenching • Microstructure • Model • Digital twin

Introduction

There is increasing importance to be able to simulate and/or predict the properties of materials in order to expedite production and also to decrease costs. If one were to know, in advance, the microstructure or material properties via some form of model, then production processes could be streamlined. Thus, a decrease in overall production costs can be

achieved. As such, a “digital twin” or computer model is an invaluable tool for modern alloy development. As one of the most commonly used magnesium alloys, AZ91 is an ideal selection to produce a model. A common practice which can help to modify the microstructures of cast materials such as Mg alloys is quenching. Changing the cooling rates of a material via quenching has been used to affect a number of microstructural features such as grain size, interdendritic arm spacing, concentration of solute in solid solution, etc. [1, 2]. By selecting four different quenching media with different cooling rates such as air, 20 °C water, 5 °C water and liquid nitrogen (LN₂) differences in the microstructure of AZ91 are expected. The AZ91 alloys are quenched immediately following casting. To generate a digital twin of the microstructure, the phase-field method has been employed. In computational materials science, this method is notably a versatile technique for simulating microstructure or interfacial evolution at the microscale. Steinbach et al. [3] pioneered such work and proposed the multi phase-field approach to capture the complete physics behind solidification and related phenomena for an arbitrary number of phases. The idea revolves around tracking the interface in space x and time t , and is represented quantitatively by the phase-field variable $\phi(x, t)$. This variable refers to the local phase fraction of a phase in N phase system and is defined in the range of $0 \leq \phi \leq 1$, where 0 and 1 point to either existence or non-existence of any representative phase while values between 0 and 1 correspond to the diffused nature of the interface between phases. The phase-field variables are constrained in such a way that the sum is unity, i.e.,

$$\sum_{\alpha=1}^N \phi_{\alpha} = 1 \quad (1)$$

This allows easy identification of all interfacial and bulk contributions. In general, the multi phase-field model introduces the total free energy density F given as:

S. Gavras (✉) · M. U. Bilal · D. Tolnai · N. Hort
 Institute of Materials Science, Helmholtz-Zentrum Geesthacht,
 Max-Planck Str. 1, Geesthacht, 21502, Germany
 e-mail: sarkis.gavras@hzg.de

$$F = \int_{\Omega} (f^{\text{chem}} + f^{\text{int}} + f^{\text{mech}} + \dots) d\Omega \quad (2)$$

F can be obtained as an integral sum of chemical free energy density f^{chem} , interfacial free energy density f^{int} and mechanical free energy density f^{mech} over the domain Ω . The first two hold vital importance for simulating solidification or growth process and other free energies like mechanical, magnetic, electrical, etc. can be added for more detailed studies. The f^{chem} and f^{int} are given as

$$f^{\text{chem}} = \sum_{\alpha=1}^N \phi_{\alpha} f_{\alpha}(c_{\alpha}) + \sum_{i=1}^{n_i} \mu^i \left[c^i - \sum_{\alpha=1}^N (\phi_{\alpha} c_{\alpha}^i) \right] \quad (3)$$

$$f^{\text{int}} = \sum_{\alpha=1, \beta \neq \alpha}^N \frac{4\sigma_{\alpha\beta}}{\eta} \left\{ -\frac{\eta^2}{\pi^2} \nabla \phi_{\alpha} \cdot \nabla \phi_{\beta} + \phi_{\alpha} \phi_{\beta} \right\} \quad (4)$$

where ϕ_{α} (or ϕ_{β}) is the phase-field variable of phase α (or β), $f_{\alpha}(c_{\alpha})$ is the chemical-free energy of phase α , μ^i is the chemical potential, c^i is the total concentration of component i , c_{α}^i is the concentration of component i in phase α and n_i is the number of components in the system. In f^{int} , $\sigma_{\alpha\beta}$ is the interfacial energy between phases α and β , and η is the interface width. Each contribution depends on various state variables passed initially as an input parameter. Substituting Eqs. 3 and 4 in Eq. 2, the kinetics of phase evolution can be written as

$$\dot{\phi}_{\alpha} = \sum_{\alpha \neq \beta}^N M_{\alpha\beta} \left[\frac{\delta F}{\delta \phi_{\beta}} - \frac{\delta F}{\delta \phi_{\alpha}} \right] \quad (5)$$

where $M_{\alpha\beta}$ is the phase-field mobility. The kinetics of diffusion of each component i is given as

$$\dot{c}^i = \nabla \cdot (D^i \nabla c^i) \quad (6)$$

here D^i is the diffusion coefficient of component i . The evolution of phase-field and concentration tracks the microstructural changes for a given set of parameters.

Experimental Methods

The alloys were cast by permanent mould indirect chill casting, described in greater detail in [4]. The composition was measured via Spark-Optical Emission Spectroscopy using an Ametek-Spectro Spectrolab M9. AZ91 ingots were quenched in air, 20 °C water, 5 °C water or liquid nitrogen from an initial temperature of approximately 700 °C. The AZ91 alloys were ground and polished using standard metallography sample preparation techniques for microstructural

investigations. In order to record polarised optical micrographs of the different samples, each sample was etched in an acetic acid, picric acid, and ethanol solution for approximately 2 s. Optical micrographs are recorded for each of the quenched samples using a Leica DMLM optical microscope using polarised light. Grain size measurements were obtained using the linear intercept method. Grain size measurements were measured from three regions from each sample and averaged to obtain grain size statistics. A TESCAN Vega3 Scanning Electron Microscope (SEM) in backscattered electron (BSE) mode was used to investigate changes to the microstructure and for qualitative compositional analysis via energy-dispersive X-ray spectroscopy (EDXS). Intermetallic area fraction measurements were obtained from five regions per quenched sample. SEM micrographs of those regions were converted to binary contrast images and ImageJ software was used to determine the area fraction of intermetallic. To produce a digital twin, simulations were performed for Mg–9Al–1Zn (wt%) in 2D (500 $\mu\text{m} \times 1 \mu\text{m} \times 500 \mu\text{m}$) in a coupled environment of two commercial tools Thermo-Calc (TQ interface) and MICRESS. As given in Eq. 1, only chemical and interfacial contributions were taken into consideration. The chemical part is responsible for the thermodynamics which is provided by Thermo-Calc on the basis of Gibbs energy data using the CALPHAD methodology [5]. On the other hand, the interfacial part takes care of how interfaces of similar and different phases behave and also controls the morphology of grains. A number of processing, material and numerical parameters needed to be initialized for setting up the model. The type of coupling in MICRESS was set to “concentration” in which the phase-field is coupled with the concentration field, and diffusion and solute partitioning are evaluated. An automatic time stepping criteria was chosen with grid spacing of 1 μm and interface width of 4 μm . In the present simulations, heterogeneous nucleation was achieved using the seed density model, i.e., allowing seeds of various radii to nucleate if the critical undercooling permits, to have an equiaxed microstructure. The model required a predefined density-radius distribution of grains and was only applied to α -Mg, while Mg₁₇Al₁₂ was set to precipitate in the interfacial regions. The temperature model with heat extraction rate as an input parameter was selected for equiaxed growth. The different cooling conditions in simulations were implemented by varying the heat extraction rate \dot{h} , i.e., high value of \dot{h} refers to high cooling rate. The extraction rates implemented in this study were $\dot{h} = 5, 15, 25$ and $35 \text{ J/cm}^3 \text{ s}$. The model assumes homogenous temperature, with no temperature gradients, which is approximated from the mean values of heat extraction rate and specific heat over the whole domain. The thermodynamic data, i.e., nucleation undercooling, driving force, solute partitioning,

diffusion coefficient/matrix, etc., are communicated by the TQ interface which is then used by the phase-field and diffusion solvers of MICRESS. The pairwise interfacial energies of phases and anisotropy parameters to exhibit hexagonal anisotropy of liquid/ α -Mg interface were adopted from the existing literature [6]. Other simulation specific numerical parameters were calibrated according to instructions mentioned in the software's manual [7]. In general, the TQ interface and four MICRESS models namely: nucleation, multi phase-field, diffusion and temperature work side by side to yield the microstructure. The simulation starts with a pure liquid phase followed by the nucleation α -Mg and afterwards with $Mg_{17}Al_{12}$ in the interdendritic regions. The simulation ends as soon as the solid fraction reaches 100%.

Results and Discussion

The composition of each AZ91 casting quenched in air, 20 °C water, 5 °C water or LN_2 is given in Table 1. In general, each casting of AZ91 has a comparable composition with the exception of the casting used to quench in 5 °C water. This casting has approximately 1 wt% more Al in comparison to the other 3 alloys cast as a result of it being the final ingot cast. This may explain, in combination with a possible higher amount of oxide (owing to it being the final casting) the greater amount of voids and inclusions present as shown in Fig. 1g. However, the compositional range of the castings given in Table 1 all still falls within the accepted margins for AZ91 alloys. Additionally, there is still sufficient surface area from AZ91 quenched in 5 °C water to perform unimpeded microstructural analysis.

In Fig. 1, the influence of different cooling rates on the microstructure, in terms of grain size and interdendritic arm spacing is apparent. It is interesting to note, however, that the grain size does not decrease proportionally with respect to the temperature of the quenching media.

The AZ91 castings left to cool in air have the largest grains and the greater interdendritic arm spacing Fig. 1a–b. It would be understandable if one would then expect the 20 °C water quenched AZ91 sample to have the next largest grain size since this is the next “warmest” quenching media. Table 2 shows quite the opposite. The AZ91 sample quenched in LN_2 (the coldest quenching medium selected,

–196 °C) has the next largest average grain size. This is due to the Leidenfrost effect [8] which occurs when an object that is significantly hotter (in this case approximately 700 °C) than the boiling point of the liquid (in this case –196 °C) come in contact. An insulating vapour is produced around the AZ91 casting, which prevents the LN_2 from rapidly quenching the material. Thus, the expected rapid cooling properties of the LN_2 are significantly reduced. Furthermore, from Table 2, both water at 20 °C and water at 5 °C are shown to be more effective quenching media with regards to average grain size reduction. The average grain size of AZ91 quenched in 5 °C water is approximately 25% of the size of grains in AZ91 quenched in air (Table 2).

The different cooling rates also have an influence on the intermetallic morphology and area fraction. Figure 2 shows micrographs of the AZ91 alloys following their respective quenching. The air quenched alloy (Fig. 2a) is composed of α -Mg, a continuous β phase, $Mg_{17}Al_{12}$ and an Al–Mn rich phase [9] (which appears brighter in the SEM micrographs).

The morphology of the intermetallic changes in the LN_2 quenched alloy from continuous to a eutectic morphology composed of β phase and α -eutectic, Fig. 2b. This structure is maintained in the 20 and 5 °C water quenched AZ91 alloys but with a lower area fraction of intermetallic. This is due to the greater amounts of solute remaining in solid solution as a result of the more rapid cooling rates [10]. Table 4 shows the decrease in intermetallic area fraction from the air quenched alloy ($7.3 \pm 1.8\%$ intermetallic) to the LN_2 and water quenched alloys (<5% intermetallic).

Digital twins generated by the phase-field model are used to comprehend the underlying physics behind solidification phenomena. Figure 3 depicts the four simulated microstructures with $\dot{h} = 5, 15, 25$ and $35 \text{ J/cm}^3 \text{ s}$. It is evident that the increasing cooling rate leads to small (or fine) grains. The grain size from the experiments appears to be exceptionally large as compared to simulations. The grain size of these twins is sensitive to parameters such as the inoculant's initial size, density, critical undercooling, shielding distance, etc. Absence of these physical parameters for nucleation makes it challenging to achieve such large grain sizes. In this regard, the simulated microstructures, in which final grain size is sensitive to the density and size of initially precipitated grains, can only be seen in terms of qualitative comparison with the experiments.

Table 1 Compositional measurements via Spark-Optical Emission Spectroscopy for each casting of AZ91 ingot

Quenching media	AZ91 Composition in wt%								
	Al	Mn	Zn	Be	Ca	Cu	Fe	Ni	Si
Air	8.99	0.23	0.67	0.00082	0.0003	0.0028	0.0007	0.0011	0.014
20 °C water	8.8	0.26	0.65	0.00092	0.0004	0.0026	0.0012	0.0011	0.015
5 °C water	9.8	0.29	0.73	0.0042	0.0005	0.0031	0.0005	<0.0002	0.0079
Liquid nitrogen	8.99	0.22	0.68	0.00078	0.0004	0.0028	0.0009	0.0011	0.015

Fig. 1 Polarised light optical micrographs of AZ91 quenched in **a–b** air, **c–d** liquid nitrogen, **e–f** 20 °C water and **g–h** 5 °C water

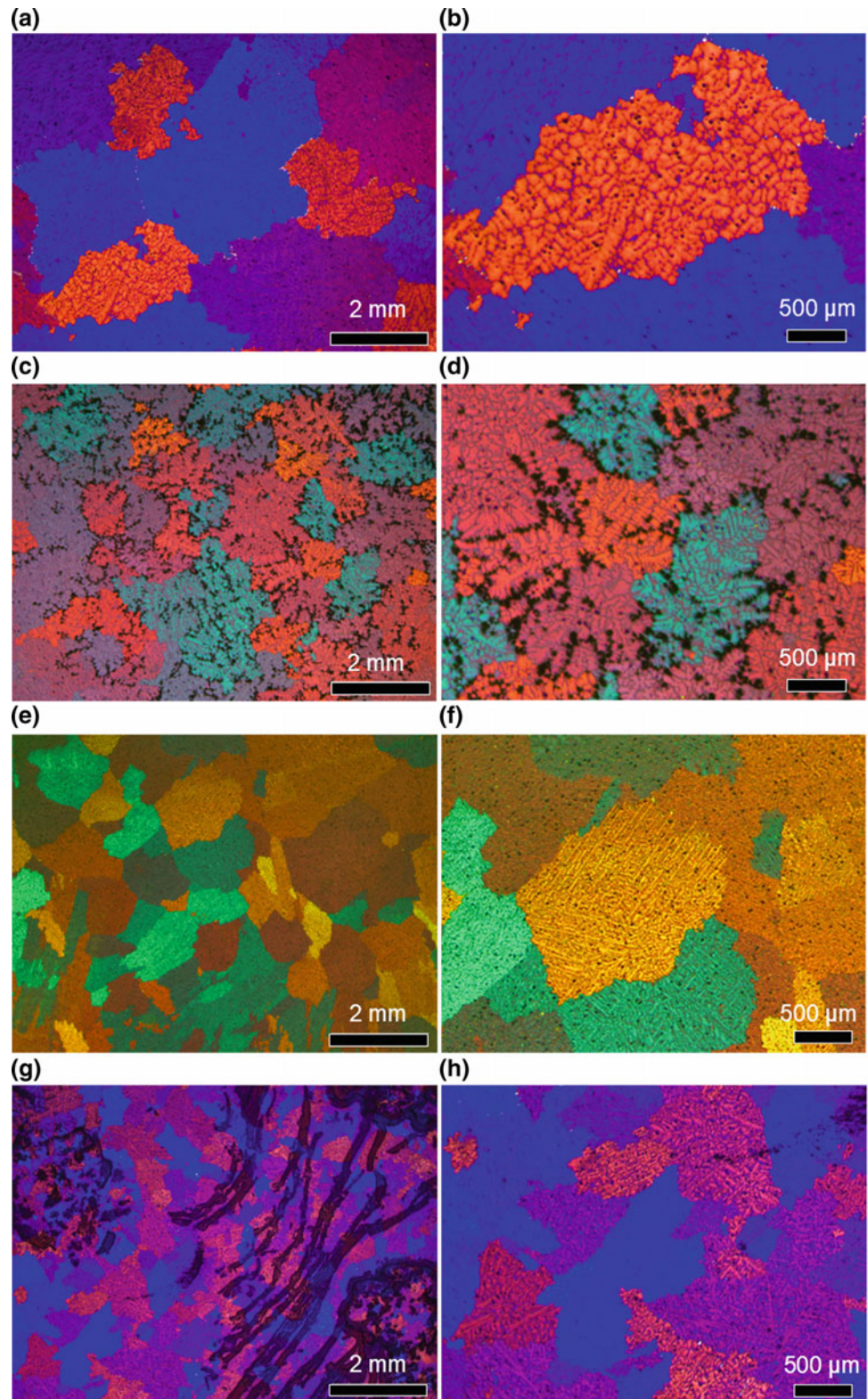
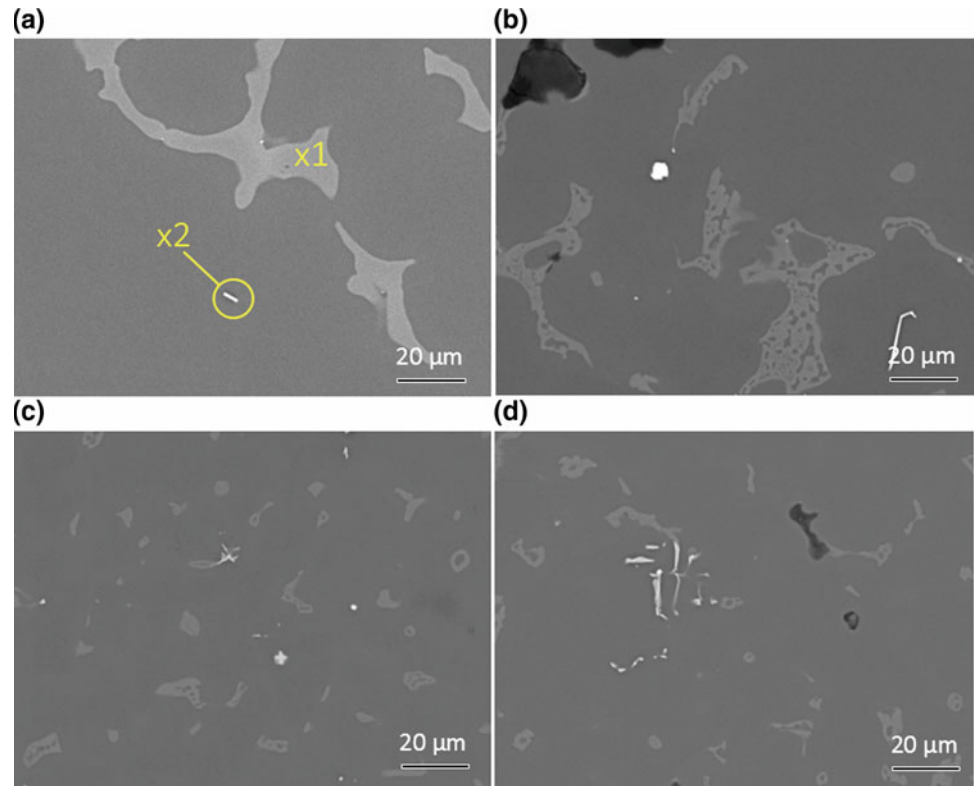


Table 2 Average grain sizes of AZ91 quenched in different media following casting

Quenching media	Average grain size \pm SD (mm)
Air	2.26 (\pm 0.16)
Liquid nitrogen	1.35 (\pm 0.13)
20 °C water	0.80 (\pm 0.08)
5 °C water	0.61 (\pm 0.05)

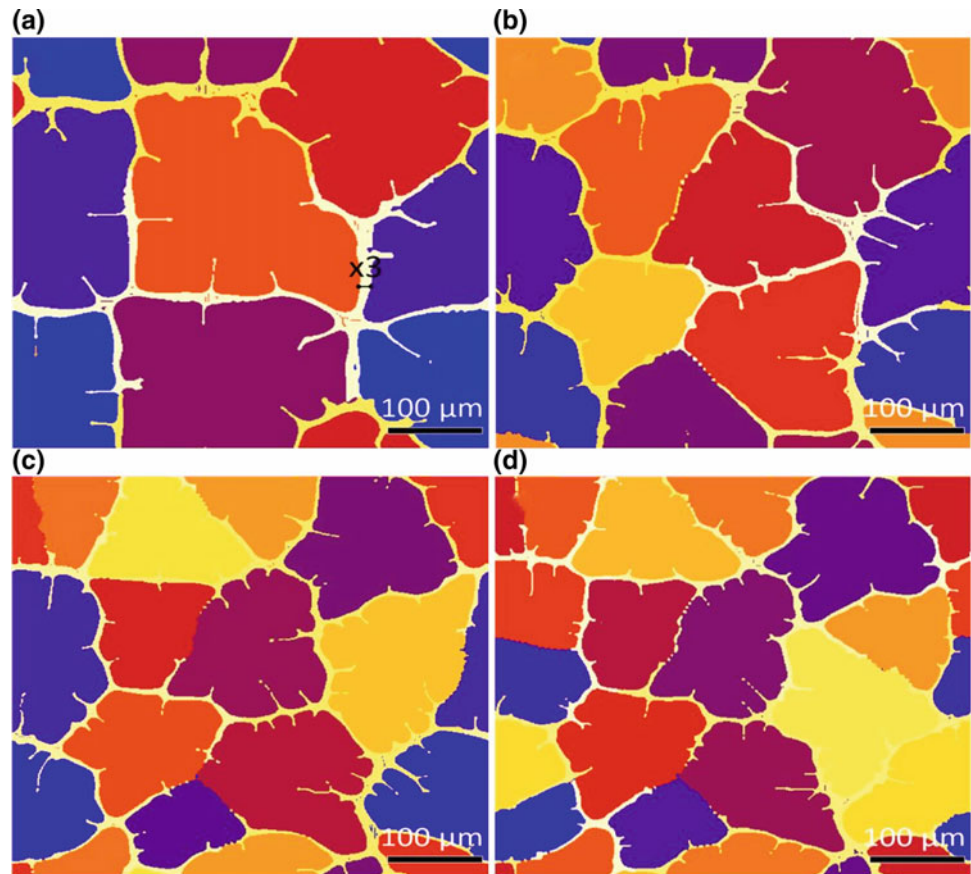
Fig. 2 Backscattered electron SEM micrographs of AZ91 quenched in **a** air, **b** liquid nitrogen, **c** 20 °C water and **d** 5 °C water. Note in **a** x1 and x2 are EDXS point measurements given in Table 3**Table 3** EDXS point scan measurements of x1 and x2 of AZ91 air quenched intermetallics shown in Fig. 2a

Element	wt%	
	x1	x2
Mg	58.3	1.6
Al	38.0	44.0
Si	0.2	0.36
Mn	0.0	54.1
Zn	3.5	0.0

Table 4 Average area fraction of intermetallic particles of AZ91 quenched in different media

Quenching media	Average area fraction \pm SD (%)
Air	7.3 (\pm 1.8)
Liquid nitrogen	4.6 (\pm 0.5)
20 °C water	4.5 (\pm 0.7)
5 °C water	3.0 (\pm 0.6)

Fig. 3 Simulated microstructures with varying cooling conditions; **a** $\dot{h} = 5 \text{ J/cm}^3 \text{ s}$, **b** $\dot{h} = 15 \text{ J/cm}^3 \text{ s}$, **c** $\dot{h} = 25 \text{ J/cm}^3 \text{ s}$ and **d** $\dot{h} = 35 \text{ J/cm}^3 \text{ s}$. Note in **a** x3 is virtual EDXS line measurement given in Fig. 4



One can also notice that the increasing heat extraction rate affects the morphology. The grains prefer to exhibit dendritic morphology rather than globular for higher values of \dot{h} . Furthermore, the grain refining effect is more pronounced as \dot{h} changes from 5 to 25 $\text{J/cm}^3 \text{ s}$. The twins are more sensitive to changes with lower values of \dot{h} than higher values, as no effective change in grain size can be observed for 25 to 35 $\text{J/cm}^3 \text{ s}$. Similar observations of grain size have been reported elsewhere in the benchmark studies of technical magnesium alloys [6].

Figure 4 represents the virtual EDXS of line x3 for microstructure $\dot{h} = 5 \text{ J/cm}^3 \text{ s}$. The concentrations of Al and Zn in the interdendritic region are similar to the one observed in experiments. The phase-field method has predicted the correct concentrations of alloying elements. It benefits in capturing the concentration kinetics/maps and can lead to insight knowledge of phenomena like solute pile-up or segregation in cases where slow diffusing elements, e.g., Mn, are involved [11]. Since simulations are performed for a ternary system, i.e., Mg, Al, and Zn, a slight difference between the experimental and modelled concentrations is possibly caused by the absence of elements which are present in the casting.

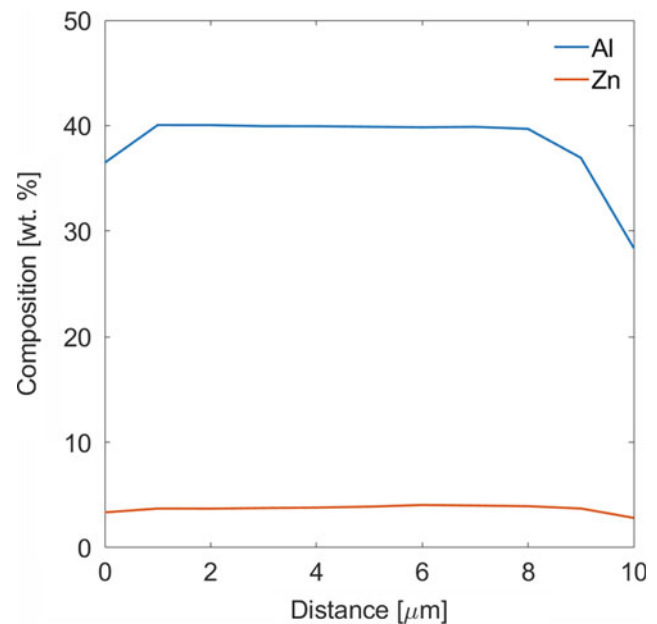


Fig. 4 Virtual EDXS line scan of the region marked as x3 in Fig. 3a

Conclusions

AZ91 cast alloys were quenched in air, 20 °C water, 5 °C water or liquid nitrogen immediately following casting. The alloy microstructures were investigated via optical and scanning electron microscopy. The AZ91 alloy left to cool in air (air quenched) had the largest average grain size. As a result of the Leidenfrost effect, the AZ91 quenched in liquid nitrogen had the next largest grain size then followed by the 20 and 5 °C water quenched alloys.

On the other hand, the phase-field simulation results are in accordance with the experiments to an extent that the varying cooling conditions yield different grain sizes. The modelled concentrations in the interdendritic region also comply with the EDXS measurement. Simulated digital twins have smaller grains as compared to the experiments due to lack of nucleation parameters. However, these twins as a preliminary attempt potentially fulfil the purpose of a qualitative comparison with the experiments and reveal a better understanding of physics behind solidification.

References

1. A.K. Dahle, Y.C. Lee, M.D. Nave, P.L. Schaffer, and D.H. StJohn: *Journal of Light Metals*, Vol. 1, (2001), p. 61.
2. M. Paliwal and I.-H. Jung: *Acta Materialia*, Vol. 61, (2013), p. 4848.
3. I. Steinbach, F. Pezzolla, B. Nestler, M. Seeßelberg, R. Prieler, G. J. Schmitz, and J.L.L. Rezende: *Physica D: Nonlinear Phenomena*, Vol. 94, (1996), p. 135.
4. F.R. Elsayed, N. Hort, M.A. Salgado Ordorica, and K.U. Kainer: *Materials Science Forum. Trans Tech Publ*, (2011), p. 65.
5. <http://www.calphad.org/>, Z.-K. Liu, Editor.
6. J. Eiken: *Int. J. Mat. Res.*, Vol. 101, (2010), p. 503.
7. www.micress.com.
8. J.G. Leidenfrost, *De aquae communis nonnullis qualitatibus tractatus*. (Ovenius, 1756).
9. I. Polmear, *Light Alloys. Materials & Mechanical Science*. (Butterworth-Heinemann, 2005).
10. F. Yavari and S.G. Shabestari: *Journal of Thermal Analysis and Calorimetry*, Vol. 129, (2017), p. 655.
11. K. Grätz, J. Eiken, and R. Schmid-Fetzer: *Int. J. Mat. Res.*, Vol. 105, (2014), p. 130.